Nucleic Acids Research Advance Access published February 20, 2015

Nucleic Acids Research, 2015 **1**
doi: 10.1093/nar/gkv123

EWS-FLI1 employs an E2F switch to drive target gene expression

Raphaela Schwentner[1,†], Theodore Papamarkou[2,†], Maximilian O. Kauer[1], Vassilios Stathopoulos[2], Fan Yang[3], Sven Bilke[3], Paul S. Meltzer[3], Mark Girolami[2] and Heinrich Kovar[1,4,*]

[1]Children's Cancer Research Institute, St. Anna Kinderkrebsforschung, Vienna 1090, Austria, [2]Department of Statistics, University of Warwick, Coventry, CV4 7AL, UK, [3]Genetics Branch, Center for Cancer Research, National Cancer Institute, Bethesda, MD 20892, USA and [4]Dept. of Pediatrics, Medical University, Vienna 1090, Austria

Received October 07, 2014; Revised February 04, 2015; Accepted February 05, 2015

ABSTRACT

Cell cycle progression is orchestrated by E2F factors. We previously reported that in ETS-driven cancers of the bone and prostate, activating E2F3 cooperates with ETS on target promoters. The mechanism of target co-regulation remained unknown. Using RNAi and time-resolved chromatin-immunoprecipitation in Ewing sarcoma we report replacement of E2F3/pRB by constitutively expressed repressive E2F4/p130 complexes on target genes upon EWS-FLI1 modulation. Using mathematical modeling we interrogated four alternative explanatory models for the observed EWS-FLI1/E2F3 cooperation based on longitudinal E2F target and regulating transcription factor expression analysis. Bayesian model selection revealed the formation of a synergistic complex between EWS-FLI1 and E2F3 as the by far most likely mechanism explaining the observed kinetics of E2F target induction. Consequently we propose that aberrant cell cycle activation in Ewing sarcoma is due to the de-repression of E2F targets as a consequence of transcriptional induction and physical recruitment of E2F3 by EWS-FLI1 replacing E2F4 on their target promoters.

INTRODUCTION

Ewing sarcoma (ES) is a highly aggressive pediatric cancer of the bone and soft tissue characterized by a gene fusion between the Ewing sarcoma gene *EWSR1* (Ewing sarcoma breakpoint region 1) and one of five alternative ETS (E twenty-six) transcription factor genes, most frequently *FLI1* (Friend leukemia virus integration site 1). The resultant oncogenic transcription factor binds DNA via the ETS DNA-binding domain and aberrantly regulates transcription of its target genes via the EWS amino terminal domain (1,2). EWS-FLI1 activated genes associate mainly with cell cycle regulation and proliferation while EWS-FLI1 repressed genes predominantly annotate to differentiation and cell communication. Promoters of EWS-FLI1 induced genes are strongly enriched in E2F motifs (3).

The E2F family of transcription factors consists of eight genes, which are transcribed in nine proteins and jointly regulate cell cycle progression (4–6). Traditionally the members are divided into transcriptional activators (E2F1–3A, B) and transcriptional repressors (E2F4-8) (6–9) though this categorization may not be as strict as originally assumed (10). E2F3b, E2F4 and E2F5 are constantly expressed throughout the cell cycle while E2F1-3a levels increase at cell cycle entry (9). Although E2F1–5 proteins comprise the same pocket protein binding domain, their interaction partners vary. E2F1–3A/B associate exclusively with pRB, while E2F4 binds to p130 and p107, and E2F5 interacts with p130 and pRB. E2F6–8 do not bind pocket proteins and act as transcriptional repressors only (8,11). E2F1–6 require dimerization with members of the differentiation-regulated transcription factor-1 polypeptide (DP) family to form functional transcription complexes on DNA. E2F7 and 8 lack a dimerization domain, but comprise tandem repeats of an E2F DNA binding domain (12,13).

Recently, we demonstrated aberrant ETS-dependent induction of E2F3 and concomitant, functionally synergistic ETS and E2F3 binding to proximal promoters of almost 50% of E2F target genes in cancers driven by ETS rearrangements, EWS-FLI1 expressing ES and TMPRSS2-ERG positive prostate cancer (14). In fact, knockdown of the chimeric ETS proteins by RNAi revealed that most E2F factors expressed in these tumors are controlled by ETS oncogenes except for E2F4, which we found constitutively expressed at high levels. Since E2F4 is considered a transcriptional repressor, we wondered if there was any kind of

*To whom correspondence should be addressed. Tel: +43 1 40470 4090; Fax: +43 1 40470 7051; Email: heinrich.kovar@ccri.at
†These authors contributed equally to the paper as first authors.

functional cross-talk between ETS induced E2F3 and E2F4 function.

MATERIALS AND METHODS

Cells and transfections

A clone of the ESFT cell line A673 with a stably transfected construct harboring a doxycyclin inducible shRNA against the EWS-FLI1 fusion protein was kindly provided by Javier Alonso (15). Cells were transfected using the Lipofectamine Plus reagent (Invitrogen, Groningen, the Netherlands).

Transcription Factor binding site analysis

Transcription factor binding site analysis was performed using ConSite (http://asp.ii.uib.no:8090/cgi-bin/CONSITE/consite).

Thymidine block

Complete Dulbecco's modified Eagle's medium (DMEM) medium with 2 mM Thymidine was added to the cells for 16 h, then the cells were washed twice with DMEM and incubated in normal DMEM for 8 h, followed by a second Thymidine block for 16 h.

Cell cycle analysis

Cell cycle analysis was performed using the Cycletest™ Plus DNA Reagent Kit (Becton Dickinson, New Jersey, USA) according to manufacturer's recommendations.

Chromatin immunoprecipitation and sequencing

Chromatin immunoprecipitation (ChIP) was performed using a ChIP-IT kit from Active Motif (Carlsbad, CA, USA), following the manufacturer's instructions with minor modifications. Briefly, A673 cells were cross-linked with 1% formaldehyde at room temperature for 15 min. Then the cells were sheared with a VirSonic 100 sonicator for 20 cycles of 10× 1-s pulses. The chromatin was immunoprecipitated overnight at 4°C. The antibody used was E2F4 (sc-866) (Santa Cruz Biotechnology, Santa Cruz, CA, USA). A mixture of Protein-G and Protein-A agarose beads was applied in pull-down experiments. After reversal of cross-linking at 65°C overnight, the ChIP DNA was purified using spin columns provided by the kit. For sequencing, the ChIP DNA was polymerase chain reaction (PCR) amplified and subsequently analyzed on an Illumina G1 Genome Analyzer (San Diego, CA, USA) following manufacturer's protocols.

Sequence reads were mapped to the human reference genome (NCBIv37, Hg19) using BWA (16) alignment program. Reads starting at identical positions, as well as low quality reads with more than two deviations from the reference or an alignment score less than 25 were removed from the resulting data sets. Local read densities were then estimated by counting coverage of read-events for each nucleotide in the genome, where the oriented reads were extended to the insert length (100 bp), which was size-selected during library preparation.

P-values were used to identify significantly increased read densities. They were estimated based on the cumulative Poisson distribution, where the local emission coefficient $\lambda(x)$ was estimated from input (non-IP) data using the average read densities of windows centered around x of sizes 1 bp, 100 bp, 1000 bp, respectively. Of those, the most conservative (largest) estimate max $\lambda_i(x)$ was used in order to minimize the false discovery rate. Discrete enriched regions were identified using the following heuristic: a continuous stretch of DNA was called significantly enriched if the following conditions were met simultaneously: $P < 10^{-9}$ anywhere within that region, and $P \leq 10^{-6}$ everywhere else. Subsequently, distinct significant regions were merged into a single region if they were less than $\frac{1}{2}$ fragment size (50 bp) apart. Finally, regions determined in this way smaller than the median fragment length (100 bp) were rejected.

Chromatin Immunoprecipitation followed by PCR

ChIP was performed using the MAGnify™ Chromatin Immunoprecipitation System (Invitrogen, Groningen, The Netherlands) according to manufacturer's instructions. Cells were cross-linked with 1% formaldehyde at room temperature for 13 min; the reaction was stopped with 125 mM Glycine for 7 min. The cells were then sheared with a Bioruptor UCD200 5 times 7 min of alternating 30 s sonication and 30 s break to achieve an average shearing size of 600 bp. Incubation times for antibody coupling and for binding chromatin to the beads were increased to 2 h and 4 h, respectively. Washing steps were extended to 20 min each. An additional washing step was introduced between IP Buffer1 and 2 using 0.1% SDS, 1% Triton X-100, 2mM EDTA, 20mMTris HCl, 500mM NaCl, pH8,1.

Following antibodies were used: anti-FLI1 antibody (MyBiosource, San Diego, California, USA, MBS300723), anti-E2F3 (Santa Cruz Biotechnology, Santa Cruz, USA sc-878), anti-E2F4 (Santa Cruz Biotechnology Inc., Santa Cruz, USA, sc-866), anti-RB (Santa Cruz Biotechnology Inc., Santa Cruz, USA, sc-50) and anti-p130 (Santa Cruz Biotechnology Inc., Santa Cruz, USA, sc-317), IgG control antibodies were from the MAGnify™ Chromatin Immunoprecipitation System (Invitrogen, Groningen, The Netherlands). Data were normalized to the input control according to the following equation: Normalized to Input = 2^(Average Ct Input – Average Ct IP). Semi-quantitative PCRs were performed using Phusion Hotstart II (Finnzymes, Espoo, Finland). Sybr Green PCR for ChIP was performed using Maxima™ SYBR Green/ROX qPCR Master Mix (Fermentas).

Primers used were:

ATAD2, 26/129: GAGCGCGGAAGAGCCAGAG and GCTGCTGCGGAGAACCACCA; -350/-240: CAGG GGTGGGGAGGAGACGC and GAGCGGTGCGTA GCCCGTTT; -1678/-1470: CCCAGACATTGCATTC TTCA and GAGGCCAATGAGAACAGAGC.

E2F3, 131/262: CCAGAGCCCCGATTATTTTT and GC AGTCGGAGTTTCCAAGTC; -123/62: CGGGTTGA GGGGCGGGGATA and TGCAACGGATTGCGAG GCGG; -272/-149: TCAAGGAGGCCTATGCAAAT and GGCCGCTACCTCCTTACTTC; -1457/-1334: AA

GGAGTCCTAGCCTGATCTGA and TGAGGATTGC AACACCTTGA.
RAD51, -51/106: ATCCGGGAGGCGGGGATACG and CAGTTCCCAGCTGCACGCCT; -186/-51: CCACCGCCCCCGGCATAAAG and CGTATC CCCGCCTCCCGGAT; -93/104: CGTCTTGGGTTA GCGCGCAG and GTTCCCAGCTGCACGCCTCG; -4270/-4017: AGGCAGGAGTATCGCTTGAA and CCATTTGAGGCCAGGAGTTA.
RAD54L 81/222: TTGGGAACAGGAAGGTTGAG and TCAGACTCAGGGAGGTCGAG; MIK67, -201/329: AGCCCTCCACTTCCTTCTTC and CGCTCCCTTC CTATTGGTC. ATAD5, 5/154: GAAGCTCTGTGGTC CGATCT and ACGGAAAGAGGCAATGAGAA

Plasmids

Promoter fragments (*E2F3*: -272/+327; *RAD51*: -186/+164) were cloned into the pGL4.10 vector (Promega).

Gene reporter assays

Cells were co-transfected with the pGL4.10-based reporter constructs and pmaxEGFP (Amaxa GmbH, Cologne, Germany) using LipofectAMINE Plus reagent (Invitrogen, Groningen, The Netherlands) at 20% density. Gene reporter assays for cells treated with Thymidine, were performed 48h after transfection using the Bright Glo Luciferase assay kit (Promega). EGFP positive cells as a measure of transfection efficiencies were monitored by standard flow cytometry.

Generation of quantitative longitudinal RNA and protein expression data for mathematical modeling

Total RNA was prepared with a Qiagen RNAeasy kit (Qiagen, Hilden, Germany). cDNA was generated from 1μg RNA (M-MLV Reverse Transcriptase, Promega, Madison, USA) and qRT-PCR performed using Maxima^{TM} SYBR Green/ROX qPCR Master Mix (Fermentas). Assays were performed in triplicate using the ABI Prism 7900 Detection System (Applied Biosystems, Foster City, CA, USA).

Relative expression levels were normalized to b-actin and analyzed by the $2^{(-\Delta\Delta Ct)}$ method (17)

Total proteins (30–50 μg) were resolved by 8.5% SDS-PAGE and processed for immunoblotting according to standard procedures. The following antibodies were used: mouse monoclonal antibody to b-actin (8226, abcam, Cambridge, UK), anti-E2F3 (Santa Cruz Biotechnology, Santa Cruz, USA sc-878) and anti-FLI1 antibody (MyBiosource, San Diego, California, USA, MBS300723). Linear protein quantification was performed using fluorescent dye coupled secondary antibodies (Dy LightTM800, Pierce Biotechnology, THP, Vienna, Austria) for detection by the LICOR Odyssey® Infrared Imaging System (LI-COR Biosciences, Bad Homburg, Germany).

Co-Immunoprecipitation

For Co-Immunoprecipitation with Ab-Crosslinking Dynabeads (Invitrogen, Groningen, The Netherlands) were incubated with the Ab over night at 4°C. After washing with 0,2M Na-Borate (pH 9,0), the beads were cross-linked with the antibody using Dimethyl pimelimidate dihydrochloride. Washing with 250 mM Tris and preelution using 0,1 M Glycine (pH 2.0); was followed by incubation of the cell lysate over night at 4°C. After washing with IP lysis buffer, elution was performed using 0,1 M Glycine (pH 2.0). The following antibodies were used: anti-E2F3 (Santa Cruz Biotechnology, Santa Cruz, USA sc-878), anti-E2F4 (Santa Cruz Biotechnology, Santa Cruz, USA sc-866), anit-RB (Santa Cruz Biotechnology, Santa Cruz, USA sc-50), anti-p130 (Santa Cruz Biotechnology, Santa Cruz, USA sc-317) and anti-FLI1 antibody (MyBiosource, San Diego, California, USA, MBS300723). Immunoblotting was performed as described above.

BAYESIAN MODEL SELECTION AND STATISTICAL METHODOLOGY

ODE formation of mechanistic models

To formulate the kinetic equations of the four models (as described in the results section) as ordinary differential equations (ODEs), some notation is introduced first. Let $\{.\}_{\{R,D,P\}}$ be the mRNA, DNA concentration and protein level of a gene, respectively. For instance, EWS_R refers to the mRNA concentration of EWS-FLI1 while $E2F3_P$ to the E2F3 protein level. Complexes are named by combining the names of their components followed by the $\{\cdot\}^C$ superscript. For example, $E2F3_P ATAD2^C_D$ denotes the complex formed by the binding of E2F3 protein on the *ATAD2* DNA. Species concentrations in ODEs are denoted as $[\{.\}_{\{R,D,P\}}]$, e.g. $[EWS_R]$ denotes the concentration of EWS-FLI1 mRNA.

The ODE representation of the system involving the formation of a dimer (model 2, Figure 4B) is provided as a representative example (the ODE representations of model 1,3 and 4 including the parameters of the models are available in the supporting material and Supplementary Tables S1, S2 and S3). The derivation of the ODE system assumes mass action kinetics. The total DNA concentration of the model consists of DNA in two forms, free and in a complex. For example, it holds for the complexes $EWS_P E2F3^C_{P,D}$ and $E2F3_D$ that

$$\frac{d\left[EWS_P E2F3^C_{P,D}\right]}{dt} = c_1 [EWS_P][E2F3_P][E2F3_D] - c_{-1} EWS_P E2F3^C_{P,D} = 0.$$

Furthermore, the total concentration $\left[E2F3^{total}_D\right]$ of $E2F3_D$ is given by

$$\left[E2F3^{total}_D\right] = [E2F3_D] + \left[EWS_P E2F3^C_{P,D}\right],$$

therefore

$$\left[EWS_P E2F3^C_{P,D}\right] = \frac{[EWS_P][E2F3_P]\left[E2F3^{total}_D\right]}{[EWS_P][E2F3_P] + \frac{c_{-1}}{c_1}}.$$

The ODE system of model 2 is then

$$\frac{d[EWS_R]}{dt} = -\hat{m}_1 [EWS_R] - d_1 [EWS_R] + a1, \quad (1)$$

$$\frac{d[EWS_P]}{dt} = t_1 [EWS_R] - d_2 [EWS_P], \quad (2)$$

$$\frac{d[E2F3_R]}{dt} = k_1 \frac{[EWS_P][E2F3_P]\left[E2F3_D^{total}\right]}{[EWS_P][E2F3_P]+\hat{c}_1} - d_3[E2F3_R], \quad (3)$$

$$\frac{d[E2F3_P]}{dt} = t_2[E2F3_R] - d_4[E2F3_P], \quad (4)$$

$$\frac{d[ATAD2_R]}{dt} = k_2 \frac{[EWS_P][E2F3_P]\left[ATAD2_D^{total}\right]}{[EWS_P][E2F3_P]+\hat{c}_2} - d_5[ATAD2_R], \quad (5)$$

where $\hat{m}_1 = m_1[shRNA]$, $\hat{c}_1 = c_{-1}/c_1$, $\hat{c}_2 = c_{-2}/c_2$. The parameters of the model and its description are provided in Table 1.

Additionally, to avoid identification problems with transcription parameters k_1,k_2 and total concentrations $\left[E2F3_D^{total}\right]$, $\left[ATAD2_D^{total}\right]$ the following reparameterisation is introduced:

$$\hat{k}_1 = k_1\widehat{\left[E2F3_D^{total}\right]},$$

$$\hat{k}_2 = k_2\widehat{\left[ATAD2_D^{total}\right]}.$$

MCMC inference

The ODEs of the mechanistic models under consideration are modeled as

$$\frac{dx}{dt} = f(x, t, \theta), x(t_1) = x_1,$$

where the derivative $d\boldsymbol{x}/dt$ of state $\boldsymbol{x}$ is, for instance, the left hand side of the ODE system (1)-(5) and $f(x, t, \theta)$ the right hand side. $\boldsymbol{x}(t)$ is the solution of the ODE for time t, and $\boldsymbol{x}_1$ are the unknown initial conditions at the starting time point t_1. All unknown parameters, including initial conditions, are collected in the vector $\boldsymbol{\theta}$. It is assumed that each observation $\boldsymbol{y}_i$, at time point t_i, $i = 1, 2, \ldots, n_t$, is a linear combination of the solution vector $\boldsymbol{x}_i$, with Gaussian additive noise $\boldsymbol{\epsilon}_i$. Since we are dealing with RNA and protein expression data with different experimental and measurement conditions, we use two distinct noise variances, v_r and v_p, to model observation noise for RNA and protein data respectively. Thus the observation model at time point t_i is of the form

$$y_{i,} = x_{i,} + \varepsilon_i, \varepsilon_{i,} \sim N(0, V),$$

where $\boldsymbol{V}$ is a diagonal matrix formed as $V = v_r I_r + v_p I_p$. $\boldsymbol{I_r}$ is an identity matrix with zeros in the diagonal elements that correspond to protein level variables, and similarly, $\boldsymbol{I_p}$ is an identity matrix with zeros in the diagonal elements which correspond to RNA expression variables. Since v_r and v_p are unknown, they are appended to the vector $\boldsymbol{\theta}$ of model parameters giving the complete parameter vector $\phi = (\theta, v_r, v_p)$.

Assuming that observations are obtained independently at each time point for each measured level, we can now use the observation model to calculate the *likelihood* of the data conditional on the model and the corresponding model parameters. Denoting the j^{th} level, $j = 1, 2, \ldots, n_s$, of the solution of the m^{th}, $m = 1, 2, 3, 4$, ODE model at time point t_i, $i = 1, 2, \ldots, n_t$, as $x_{ij}^{(m)}\left(\theta^{(m)}\right)$ with the corresponding model parameters $\theta^{(m)}$, the *likelihood* for model M_m is

$$p\left(Y|\phi^{(m)}, M_m\right) = \prod_{i=1}^{n_t}\prod_{j=1}^{n_s} \mathbf{1}_{ij} N(y_{ij}|x_{ij}^{(m)}\left(\theta^{(m)}\right), v_{ij}).$$

The experimental data described earlier correspond to the observation matrix $\boldsymbol{Y}$ of the statistical model and are available in the supporting material (Supplementary Figure S4). The indicator fucntion $\mathbf{1}_{ij}$ accounts for missing data. If level j has been measured at time point t_i, then $\mathbf{1}_{ij} = 1$. On the other hand, if an experimental observation has not been made at time point t_i for species j, then $\mathbf{1}_{ij} = 0$. v_{ij}denotes the $(i,j)^{th}$ element of noise variance matrix V.

For comparing different models, e.g M_1 versus M_2, assuming that all models are *a-priori* equally probable we need to calculate the *Bayes factor*

$$\frac{p(Y|M_1)}{p(Y|M_2)} = \frac{\int p\left(Y|\phi^{(1)}, M_1\right) p(\phi^{(1)}|M_1)d\phi^{(1)}}{\int p\left(Y|\phi^{(2)}, M_2\right) p(\phi^{(2)}|M_2)d\phi^{(2)}}, \quad (6)$$

where $p(\phi^{(1)}|M_1)$ is the prior distribution for the parameters of the corresponding model. The integrals in equation (6) are the *marginal likelihoods* of the models which are calculated using Markov Chain Monte Carlo by sampling from the *posterior* distribution of the parameters $p\left(\phi^{(m)}|Y, M_m\right)$. Due to the non-linear dependence of the ODE models on the parameters the *posteriors* exhibit multiple local maxima and strong correlations. Therefore we employ a population MCMC sampler for sampling from 50 power posteriors (18) with a simplified Manifold Metropolis-Adjusted Langevin Algorithm [simplified MMALA see (19)]. Population MCMC allows the algorithm to sample between different local maxima while the simplified MMALA allows for efficient sampling under strong correlation regimes. More details on the implementation of the MCMC inferential scheme can be found in the 'Supplements'. Previous work in systems biology as exemplified by (20) has employed similar mechanistic models formed by systems of ODEs to study gene regulatory networks with great success. In (20) however, the models were scored by carefully constructing functions measuring how the models fit several aspects of the data and optimizing the model parameters. In our work we construct a Bayesian model selection framework by using Bayes factors computed by properly marginalizing all model parameters and associated uncertainty out of the models. The methodology presented in this paper is more similar to the work in (21).

RESULTS

E2F4 co-localization with E2F3 and EWS-FLI1

To compare E2F3 and E2F4 binding patterns in ES, E2F4 specific ChIP-seq was performed on the same A673 ES cell line-derived chromatin previously used in EWS-FLI1 and E2F3 specific pull-down experiments (14). In brief, after preprocessing 12.7 Mio. reads were uniquely aligned to the human genome (hg19) corresponding to 1816 distinct genomic E2F4 binding regions [all alignment/peak-finding parameters essentially as in (14)]. Of these 1816 peaks, 1151

Table 1. Parameters and description for model 2

Parameter	Description
a_1	EWS-FLI1 transcription rate times EWS-FLI1 DNA concentration
m_1	shRNA mediated degradation rate constant of EWS mRNA
d_1	EWS-FLI1 mRNA degradation rate constant
t_1	EWS-FLI1 translation rate constant
d_2	EWS-FLI1 protein degradation rate constant
k_1	EWS-FLI1 mediated E2F3 transcription rate constant
c_1	EWS-FLI1 E2F3 association rate constant
c_{-1}	EWS-FLI1 E2F3 disassociation rate constant
k_2	Complex ATAD2 transcription rate constant
c_2	E2F3 protein E2F3 DNA association rate constant
c_{-2}	E2F3 protein E2F3 DNA disassociation rate constant
d_3	E2F3 mRNA degradation rate constant
t_2	E2F3 translation rate constant
d_4	E2F3 protein degradation rate constant
d_5	ATAD2 mRNA degradation rate constant

and 1159 (63.4% and 63.8%) overlapped with E2F3 and EWS-FLI1 peaks, respectively. Importantly, 854 (46.9%) showed concomitant EWS-FLI1, E2F3 and E2F4 binding (Figure 1A). Similar results were obtained using an alternative peak calling strategy (MACS2) as described in the supporting material. Here, E2F4 frequently occupied exactly the same binding sites in aberrant ETS/E2F regulated promoters as E2F3 (Supplementary Figure S1) suggesting a binding competition between the two counteracting E2F factors. Since binding of EWS-FLI1 or TMPRSS2-ERG to these promoters is associated with gene activation (14), we studied the influence of EWS-FLI1 modulation on quantitative E2F3 and E2F4 occupation of selected target promoters (*E2F3, ATAD2, RAD51*) by semi-quantitative and real-time quantitative ChIP-qPCR before and at different time points after induced EWS-FLI1 silencing in A673 ES cells carrying doxycycline controllable EWS-FLI1 shRNA (15).

For the *E2F3* gene, three areas of EWS-FLI1/E2F3 binding were investigated at (-272/-149), (-123/62) and (131/262) relative to the transcription start site (TSS). As negative control, an upstream region (-1457/-1334) devoid of ETS and E2F recognition sites was used. In the presence of the oncogene, ChIP assays revealed strong binding of E2F3 but weak binding of E2F4 to all three tested promoter sites. With increasing time after the induction of EWS-FLI1 knockdown, *E2F3* promoter occupancy by E2F3 decreased while E2F4 binding increased. This replacement of E2F3 by E2F4 on the *E2F3* promoter occurred gradually over time with a complete exchange 48h after knockdown of EWS-FLI1 (Figure 1B and E). The binding pattern of E2F3 and E2F4 on the *ATAD2* (Figure 1C and F) and *RAD51* (Figure 1D and G) promoters resembled the *E2F3* promoter occupancy with decreasing E2F3 binding and increasing E2F4 binding after knockdown of EWS-FLI1. Negative control regions in the three tested promoters showed significantly less E2F3 and E2F4 binding. In addition, promoters of three EWS-FLI1 activated genes, bound by E2F3 and E2F4, but, according to ChIP-seq, not EWS-FLI1, were investigated before and after knockdown of the oncogene. While E2F3 binding decreased slightly on two of the three promoters (*MKI67* and *RAD54L*) upon EWS-FLI1 modulation, E2F4 was already bound to the promoters before

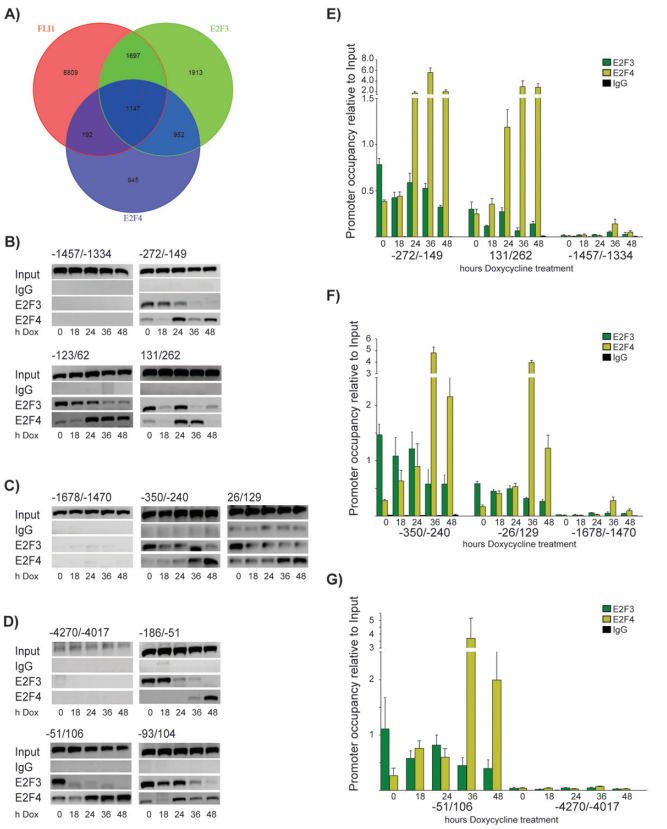

Figure 1. E2F3 and E2F4 binding to target promoters: (**A**) Venn diagram of gene numbers associated with E2F3, E2F4 or EWS-FLI1 binding in A673 cells and their overlaps. Binding data for EWS-FLI1 and E2F3 are taken from (14). (**B**–**D**) ChIP-PCR and (**E**–**G**) quantitative longitudinal ChIP-qPCR results for three EWS-FLI1 target genes before and at different time points after induction of EWS-FLI1 silencing. Cells were either left untreated (0) or were treated with doxycycline for 18, 24, 36 and 48h. E2F3 (dark green) and E2F4 (light green) ChIPs were followed by PCR amplification of genomic regions containing putative E2F binding sites. For control, gene regions far upstream of the TSS of the corresponding genes devoid of E2F or ETS binding sites were used. *E2F3* (B and E), *ATAD2* (C and F) and *RAD51* (D and G). For control, ChIP using unrelated IgG was performed. Y axis: Promoter occupancy relative to Input. Results are means ± SD from a representative experiment performed in at least triplicates.

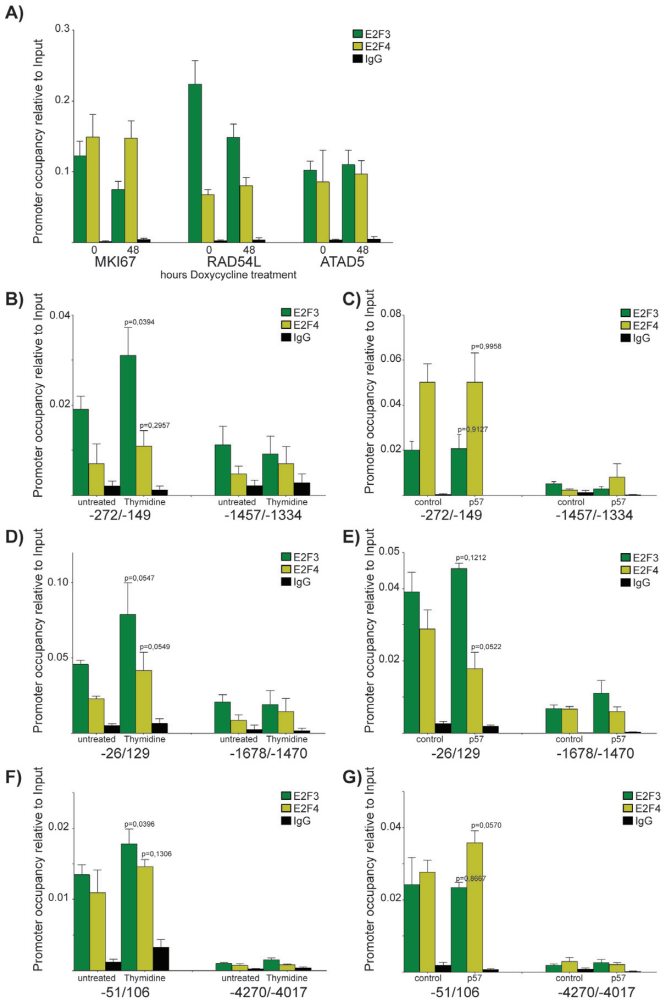

Figure 2. E2F binding is dependent on EWS-FLI1 and independent of cell cycle. (**A**) E2F3 (dark green) and E2F4 (light green) promoter occupancy was analyzed by ChIP-qPCR on three promoters (MKI67, RAD54L and ATAD5) identified by ChIP-seq to be bound by E2F3 and E2F4, but not EWS-FLI1, before (0) and after (48) doxycycline induced knockdown of EWS-FLI1. (**B**–**G**) Cells were either left untreated (untreated /control), or treated with thymidine (B, D and F) or were transfected with a p57 expression plasmid (C, E and G), and ChIP-qPCR was performed with antibodies to E2F3 (dark green) and E2F4 (light green) as well as unrelated IgG for negative control. Regions for *E2F3* (B, C), *ATAD2* (D,E) and *RAD51* (F, G) containing putative E2F binding sites and corresponding control regions without binding sites were amplified. Y axis: Promoter occupancy relative to Input. Results are means ± SD from a representative experiment performed in triplicates.

and not further increased after knockdown of EWS-FLI1 on all three tested promoters (Figure 2A). These results suggest that on EWS-FLI1 occupied promoters, depletion of the oncogene leads to a gradual replacement of activating E2F3 by repressive E2F4, which is not observed on E2F3 regulated promoters lacking EWS-FLI1 binding.

For several genes, regulation by E2F factors was previously demonstrated to be cell cycle dependent (11). Since knockdown of EWS-FLI1 in ES induces cell cycle arrest [(22) and Supplementary Figure S2A)], we tested whether the observed E2F3/E2F4 exchange upon inducible EWS-FLI1 knockdown might be the consequence or the cause of cell cycle attenuation. We employed, two different established strategies to arrest A673 cells in G1 in the presence of EWS-FLI1, double thymidine blockade and ectopic expression of p57 (CDKN1C/KIP2) (23,24). These experimental settings resulted in similar proportions of cells arrested in G1 as induced by EWS-FLI1 knockdown (Supplementary Figure S2A), but did not affect EWS-FLI1 expression (Supplementary Figure S2B). Importantly, neither thymidine blockade nor forced p57 expression reduced E2F3 binding or significantly increased E2F4 occupancy of the *E2F3*, *ATAD2* and *RAD51* promoters (Figure 2B–F). In addition, although knockdown of EWS-FLI1 markedly reduces promoter activity of *E2F3* and *RAD51* genes in luciferase reporter assays (14), no difference in promoter activities of these genes was observed between control and thymidine block conditions (Supplementary Figure S2C).

Taken together these results confirm that the replacement of E2F3 by E2F4 and the modulation of target promoter activities upon EWS-FLI1 knockdown is not a mere consequence of induced cell cycle arrest but causally related to the presence/absence of EWS-FLI1. We therefore hypothesized that in the presence of EWS-FLI1 E2F3 is transcriptionally activated and recruited to EWS-FLI1/E2F3 co-regulated promoters to replace constitutively expressed repressive E2F4.

Pocket proteins reflect binding patterns of their E2F interaction partners

Pocket protein binding to E2Fs plays a critical role in cell cycle regulation. E2F3 forms a complex with pRB and E2F4 with p130 (25,26). We therefore interrogated the binding patterns of pRB and p130 to EWS-FLI1/E2F regulated promoters by quantitative ChIP-PCR (Figure 3). Although absolute signal intensities varied between different promoters indicative of variable affinities, pRB binding to the various tested promoters was generally reduced upon knockdown of EWS-FLI1 as was binding of its interaction partner E2F3. In contrast, binding of p130 in combination with E2F4 increased after EWS-FLI1 depletion. These findings indicate that E2F3 and E2F4 bind to EWS-FLI1 regulated genes as complexes with pRB and p130, respectively.

Together, our results indicate that in the presence of EWS-FLI1, E2F target promoters are occupied by the transcriptionally activating E2F3/pRB complex. In the absence of EWS-FLI1, this complex is replaced by the repressive E2F4/p130 complex. Since E2F4 and p130 are constitutively expressed these data support a model in which EWS-FLI1 binding leads to dissociation of E2F4/p130 from and recruitment of E2F3/pRB to their shared target promoters suggesting an active regulatory role of EWS-FLI1 in cooperative promoter activation by E2F3.

This may be best explained by a direct physical interaction of the EWS-FLI1 protein with any of the E2F/pocket protein complexes. In order to test for interaction between EWS-FLI1 and the different E2F/pocket protein components, we performed co-immunoprecipitation experiments (Co-IP) followed by immunoblot analyses. While E2F/pocket protein complexes were readily detectable, no experimental evidence for physical interaction between EWS-FLI1 and E2F/pocket protein pull-down products

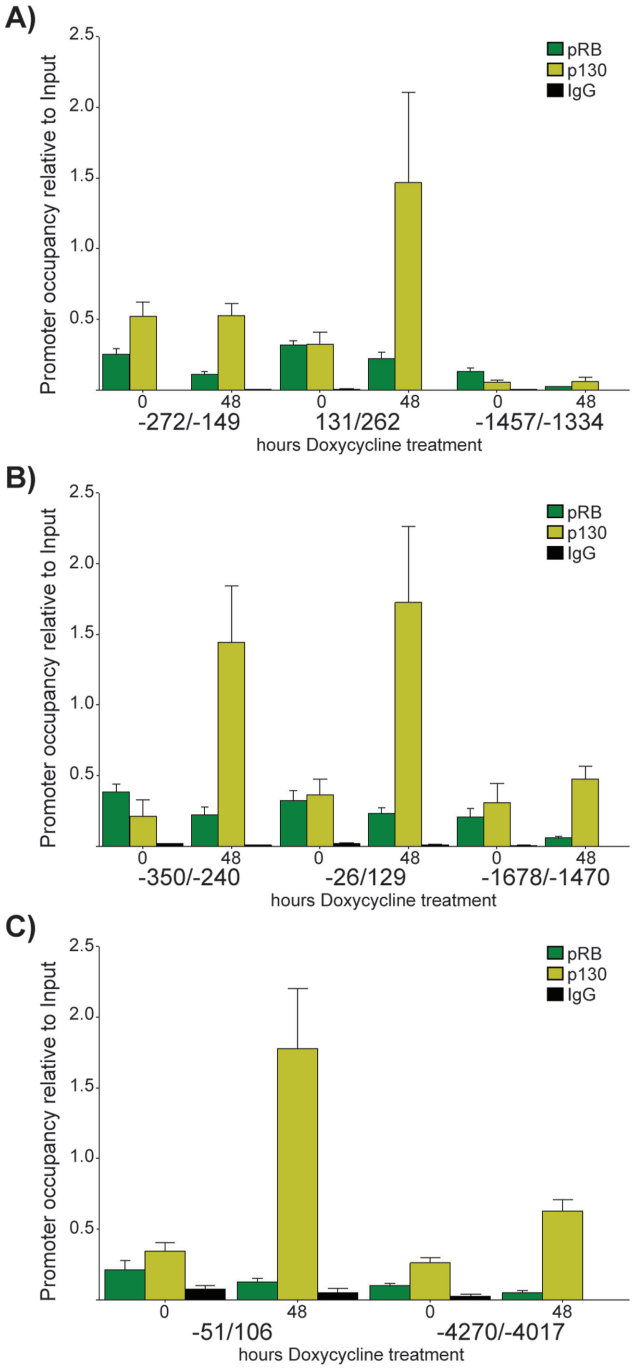

Figure 3. Pocket proteins reflect binding patterns of their E2F interaction partners: ChIP assays were performed in A673 ESFT cells. Cells were either left untreated (0) for control, or were treated for 48h with doxycycline to induce knockdown of EWS-FLI1. pRB (dark green) and p130 (light green) ChIPs were followed by qPCR amplification of promoter regions containing ETS and/or E2F sites, and, for negative control, a region upstream of the corresponding TSS not containing E2F or ETS binding sites for (**A**) *E2F3*, (**B**) *ATAD2* and (**C**) *RAD51*. For control, ChIP using unrelated IgG was performed. Y-axis: Promoter occupancy relative to Input. Results are means ± SD from a representative experiment performed in at least triplicates.

was obtainable (Supplementary Figure S3). This result may either be explained by a lack of complex formation between the ES oncoprotein and E2F factors. Alternatively, the co-occurrence of E2F3 and E2F4 on the same promoter sites in the presence of EWS-FLI1 in ChIP experiments may reflect heterogeneity across the cell population which would be expected to be observed in case of a high on/off rate of E2F transcription factor binding.

Bayesian model selection

So far our data strongly suggested functional synergy between E2F3 and EWS-FLI1 in the activation of their shared targets via a EWS-FLI1 induced E2F4/E2F3 exchange mechanism. In the absence of experimental evidence for a physical complex between EWS-FLI1 and any of the E2F complex components, we decided to take a statistical modeling approach based on longitudinal quantitative measurements of *EWS-FLI1*, *E2F3*, *ATAD2 and RAD51* gene expression to explain the observed functional synergy. EWS-FLI1 and E2F3 protein levels were determined by fluorescent immunoblots, and RNA expression was analyzed by qRT-PCR using primers amplifying *EWS-FLI1*, *E2F3*, *ATAD2* and *RAD51* and normalized to *b-actin* expression. Samples were analyzed at 0, 10, 15, 18, 21, 24, 27, 30, 33, 36, 39, 42, 45 and 48 h of doxycycline treatment.

E2F4 was excluded from the modeling approach, as RNA and protein levels are not changing upon knockdown of EWS-FLI1 and therefore would not provide additional information. Furthermore in the statistical modeling part of this work, we were mainly interested in the mechanism how EWS-FLI1 and E2F3 are regulating their shared target genes.

The data used in the statistical analysis are available in the supporting material (Supplementary Figure S4). Furthermore, the data as well as the accompanying MATLAB code have been made publicly available as a git repository at https://github.com/UniversityofWarwick/ews_fli1_and_e2f_nar_article.

Description of mechanistic models

Bayesian model selection was used in order to answer whether EWS-FLI1 and E2F3 proteins activate their shared target genes independently or synergistically, exemplified by *ATAD2* and validated with *RAD51*. First, four candidate mechanistic models describing possible scenarios for the regulation of *ATAD2* were constructed.

Figure 4 visualizes the mechanisms behind these four models. Model 1 assumes that the EWS-FLI1 and E2F3 proteins independently target genes including *E2F3* itself. Model 2 postulates that target gene transcription depends on the co-binding of EWS-FLI1 and E2F3 proteins as a complex or separately but in interdependence. Model 3 presumes EWS-FLI1 protein activates transcription of target genes alone without a contribution of E2F3. Finally, model 4 supposes that the EWS-FLI1 protein first activates the transcription of *E2F3*, and E2F3 protein subsequently activates transcription of target genes.

It is noted that finer possible adaptations in the modeling of regulation of E2F3 target genes may provide varia-

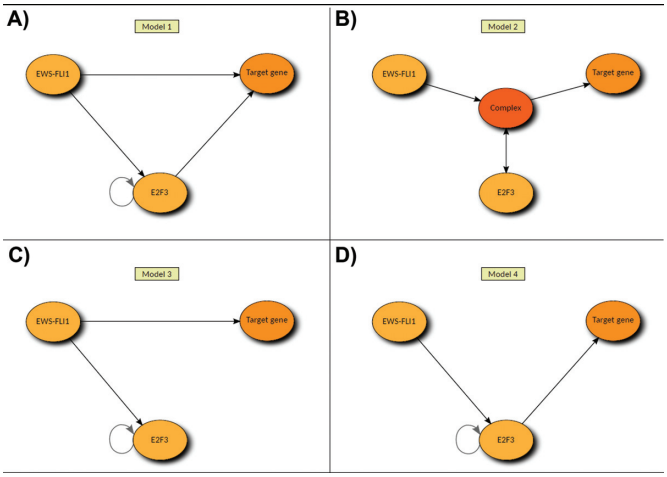

Figure 4. Candidate models for the regulation of E2F target genes by EWS-FLI1. (**A**) Model1: EWS-FLI1 activates E2F3, and target gene transcription is regulated independently by EWS-FLI1 and E2F3. EWS-FLI1 and E2F3 independently bind on E2F targets. (**B**) Model2: EWS-FLI1 and E2F3 synergistically activate transcription. (**C**) Model3: Target gene activation is exclusively driven by EWS-FLI1 with no contribution of E2F3. (**D**) Model4: Target gene activation is driven exclusively by E2F3, and EWS-FLI1 regulates target gene expression indirectly through induction of E2F3.

tions of the four candidate mechanistic models. Experimental and computational limitations have been factored in at the stage of model construction in an attempt to establish a representative set of the broad spectrum of plausible modeling configurations.

The four mechanistic models can be described by systems of ODEs parameterized by unknown kinetic parameters. All models comprise five states corresponding to the mRNA concentrations and protein levels of EWS-FLI1, E2F3 and the mRNA concentrations of the target gene. *ATAD2* was used as the primary model target gene. The analysis was subsequently rerun using *RAD51* as the target to provide reinforcing evidence in favor of the selected model.

The specifics of ODE formation and of MCMC inference are treated in the 'Methods' section of the paper, while associated technical details are exposed more elaborately in the supporting material.

Statistical outcome

The four candidate models have been compared on the statistical basis of the inferred Bayes factors, which in turn have been computed using the log-marginals derived via MCMC inference, see equation (S21) in the supporting material. It is noted that the observation matrix $\boldsymbol{Y}$ appearing in equation (S21) corresponds to the experimental data, which are visualized in Figure S4.

Table 2 displays the Bayes factors for the four models after running the analysis twice, once using *ATAD2* and once using *RAD51* as the target gene. In both cases, the order of the Bayes factors across the four models is preserved. Model 2 is the most probable one among the four candidate models irrespectively of the target gene data (*ATAD2* or *RAD51*) employed in the simulations. This confirms the model of a synergistic regulation of E2F3 target genes by EWS-FLI1

Table 2. Bayes factors for the four mechanistic models using ATAD2 and RAD51 as target genes

Model	E2F3 Target Gene	
	ATAD2	RAD51
1	0.65%	1.46%
2	**97.35%**	**87.83%**
3	1.88%	10.58%
4	0.13%	0.12%

and E2F3. Supplementary Figures S5 and S6 in the supporting material show how model 2 fits the observed data by using multiple simulations of the ODE system with parameters sampled from the posterior distribution. The posterior means for the two noise variances, v_r and v_p, where 0.0111 and 0.0088 for the *ATAD2* target gene and 0.0149, 0.0078 for the *RAD51* target gene.

DISCUSSION

A major hallmark of oncogenesis is the deregulation of cell cycle genes in order to promote proliferation of cancer cells (27). In ES, EWS-FLI1 binds to and activates the promoters of several cell cycle regulators, in particular of E2F transcription factor genes including *E2F3,* and silencing of EWS-FLI1 induces cell cycle arrest. Our previous data suggested a feed-forward loop activation of E2F3 and of at least 50% of E2F3 target genes by combinatorial binding of EWS-FLI1 and E2F3 (14,28). However, the molecular mechanism behind synergistic EWS-FLI1/E2F target gene activation remained unknown. In this study we analyzed the co-localization and binding dynamics of EWS-FLI1 and E2F factors to selected promoters and applied mathematical modeling as an approach to better understand the functional synergy between oncogenic ETS and the cellular E2F dependent gene regulatory network. As the bona fide progenitor cell type for ES remains controversial (3,29–32) we chose to use a tightly controllable EWS-FLI1 knockdown system in ES cells as a reverse model to infer the basis of EWS-FLI1/E2F3 synergy. We found that the drop in target gene expression upon knockdown of EWS-FLI1 is accompanied by loss of E2F3/pRB and gain of E2F4/p130 occupancy at target promoters. This E2F exchange was not a consequence of EWS-FLI1 knockdown-induced cell cycle arrest but exclusively related to and presumably caused by altered availability of EWS-FLI1. Since E2F3 expression levels vary with the availability of EWS-FLI1, one possible mechanistic explanation for the replacement of E2F3/pRB by E2F4/p130 complexes on E2F target promoters upon EWS-FLI1 knockdown is competitive binding driven by changes in relative E2F3 and E2F4 concentrations. In this case, the expression of EWS-FLI1/E2F target genes is solely dependent on E2F3 binding but not on EWS-FLI1 promoter occupation (model 4 in Figure 4). However, our mathematical modeling approach excluded this possibility, with a Bayes factor <0.2% (Table 2). In fact, our promoter ChIP-PCR data for EWS-FLI1 regulated E2F target genes lacking EWS-FLI1 binding demonstrated that the mere reduction in E2F3 levels as a consequence of EWS-FLI1 knockdown was not sufficient to al-

ter E2F4 promoter occupancy which contrasts EWS-FLI1 binding promoters. Also, we excluded the possibility that EWS-FLI1 acts as a mere hijacker of E2F target genes activating them independently of E2F3/pRB binding and activity (models 1 and 3 of Figure 4). The fact that the model postulating EWS-FLI1 as the only relevant activator of EWS-FLI1/E2F target genes (model 3) was slightly more probable than the model proposing co-regulation by independent promoter binding of EWS-FLI1 and E2F3 (model 1; Bayes factors 1.88 and 10.58 for *ATAD2* and *RAD51*, respectively, versus 0.46 and 1.65) might already indicate a dominant role of EWS-FLI1 as a driver of E2F target gene activation. However, the by far most probable model (model 2 in Figure 4; Bayes factor 97.35 and 87.83 for *ATAD2* and *RAD51*, respectively) predicts synergy either through physical and/or functional interaction between EWS-FLI1 and an E2F3 complex as a necessary prerequisite for combinatorial promoter binding and activation. It is in accordance with our previously published observations that mutation of the ETS binding motif prevents E2F3 binding, while mutation of the E2F site does not affect EWS-FLI1 occupation of their shared target promoters, and that the frequency of co-occurrence of EWS-FLI1 and E2F3 binding in promoter regions is significantly more frequent than expected by chance (14). These results suggest that, when present, EWS-FLI1 not only induces but also recruits activating E2F3/pRB complexes to promoters which, in the absence of EWS-FLI1, are restrained by repressive and constitutively expressed E2F4/p130 complexes.

In support of our model, Freedman *et al*. demonstrated in a glioblastoma cell line for the Cdc6 promoter that activating and repressive E2Fs can bind to the same site, and that the interaction with co-factors binding to DNA motifs in the vicinity determines the fate of target gene expression by selecting for activating E2F3 instead of E2F4 (33). Similarly, in prostate stromal cells, androgen receptor (AR) physically interacts with E2F1 in gene activation, although this interaction was independent of androgen binding and no evidence for the involvement of pocket proteins was obtained (34). EWS-FLI1 may represent another such example functionally interacting with an activating E2F factor. However, we were unable to experimentally demonstrate protein interaction between EWS-FLI1 and E2F3/pRB complexes.

Several reasons may account for this deficiency. Among them are low affinity and high turn-over binding, or dependence on chromatin structure. Since the N-terminal region of EWS-FLI1 was demonstrated to associate with HDAC1 (35), it is also possible that EWS-FLI1/E2F3 communication occurs through a transient interaction with the repressive pRB/E2F3/HDAC1 complex leading to complex disruption and the release of active E2F3 eventually inducing target gene expression (36). The systems biology approach applied in this study enabled us to overcome the bottleneck in experimental evidence. Based solely on time resolved RNA and protein expression data we were able to clearly select an explanation model for EWS-FLI1 dependent empirical target expression kinetics. More sensitive methods are likely necessary to experimentally consolidate this model. Bimolecular fluorescence complementation assays could be used to validate the interaction of EWS-FLI1 with E2F factors and/or pocket proteins. Affinity purification coupled to mass spectrometry to detect interaction partners would be an alternative option. However, due to the intrinsically disordered nature of EWS-FLI1, this approach may not be successful (37). Furthermore singe cell studies to follow the exchange would be useful to exclude heterogeneity of the cell population.

In summary, an integrative analysis and mathematical modeling of time resolved gene expression and ChIP data for EWS-FLI1, E2F3, E2F4 and two target genes revealed that EWS-FLI1 facilitates E2F3/pRB recruitment to target genes that are otherwise restrained by repressive E2F4/p130 complexes. This study provides an excellent example for the power of systems biology in the study of complex gene regulatory mechanisms that are otherwise difficult to assess experimentally.

SUPPLEMENTARY DATA

Supplementary Data are available at NAR Online.

ACKNOWLEDGEMENT

The authors thank Dieter Printz for FACS analysis and Alexander Boro for technical advice concerning the additional ChIP washing buffer.

FUNDING

Austrian Science Fund (FWF) [22328-B09]; 7th framework program of the European Commission [259348] (ASSET). DOC-fFORTE fellowship of the Austrian Academy of Sciences [to R.S.]. Funding for open access charge: 7th framework program of the European Commission [259348] (ASSET).
Conflict of interest statement. None declared.

REFERENCES

1. Kovar,H. (2010) Downstream EWS/FLI1 - upstream Ewing's sarcoma. *Genome Med.*, **2**, 8.
2. Bernstein,M., Kovar,H., Paulussen,M., Randall,R.L., Schuck,A., Teot,L.A. and Juergens,H. (2006) Ewing's sarcoma family of tumors: current management. *Oncologist*, **11**, 503–519.
3. Kauer,M., Ban,J., Kofler,R., Walker,B., Davis,S., Meltzer,P. and Kovar,H. (2009) A molecular function map of Ewing's sarcoma. *PLoS One*, **4**, e5415.
4. Crosby,M.E. and Almasan,A. (2004) Opposing roles of E2Fs in cell proliferation and death. *Cancer Biol. Ther.*, **3**, 1208–1211.
5. Hallstrom,T.C. and Nevins,J.R. (2009) Balancing the decision of cell proliferation and cell fate. *Cell Cycle*, **8**, 532–535.
6. Polager,S. and Ginsberg,D. (2009) p53 and E2f: partners in life and death. *Nat. Rev. Cancer*, **9**, 738–748.
7. Chen,H.Z., Tsai,S.Y. and Leone,G. (2009) Emerging roles of E2Fs in cancer: an exit from cell cycle control. *Nat. Rev. Cancer*, **9**, 785–797.
8. Swiss,V.A. and Casaccia,P. (2010) Cell-context specific role of the E2F/Rb pathway in development and disease. *Glia*, **58**, 377–390.
9. Danielian,P.S., Friesenhahn,L.B., Faust,A.M., West,J.C., Caron,A.M., Bronson,R.T. and Lees,J.A. (2008) E2f3a and E2f3b make overlapping but different contributions to total E2f3 activity. *Oncogene*, **27**, 6561–6570.
10. Chong,J.L., Wenzel,P.L., Saenz-Robles,M.T., Nair,V., Ferrey,A., Hagan,J.P., Gomez,Y.M., Sharma,N., Chen,H.Z., Ouseph,M. *et al.* (2009) E2f1–3 switch from activators in progenitor cells to repressors in differentiating cells. *Nature*, **462**, 930–934.

11. Takahashi,Y., Rayman,J.B. and Dynlacht,B.D. (2000) Analysis of promoter binding by the E2F and pRB families in vivo: distinct E2F proteins mediate activation and repression. *Genes Dev.*, **14**, 804–816.
12. Cam,H., Balciunaite,E., Blais,A., Spektor,A., Scarpulla,R.C., Young,R., Kluger,Y. and Dynlacht,B.D. (2004) A common set of gene regulatory networks links metabolism and growth inhibition. *Mol. Cell*, **16**, 399–411.
13. van den Heuvel,S. and Dyson,N.J. (2008) Conserved functions of the pRB and E2F families. *Nat. Rev. Mol. Cell Biol.*, **9**, 713–724.
14. Bilke,S., Schwentner,R., Yang,F., Kauer,M., Jug,G., Walker,R.L., Davis,S., Zhu,Y.J., Pineda,M., Meltzer,P.S. *et al.* (2013) Oncogenic ETS fusions deregulate E2F3 target genes in Ewing sarcoma and prostate cancer. *Genome Res.*, **23**, 1797–1809.
15. Carrillo,J., Garcia-Aragoncillo,E., Azorin,D., Agra,N., Sastre,A., Gonzalez-Mediero,I., Garcia-Miguel,P., Pestana,A., Gallego,S., Segura,D. *et al.* (2007) Cholecystokinin down-regulation by RNA interference impairs Ewing tumor growth. *Clin. Cancer Res.*, **13**, 2429–2440.
16. Li,H. and Durbin,R. (2009) Fast and accurate short read alignment with Burrows-Wheeler transform. *Bioinformatics*, **25**, 1754–1760.
17. Schmittgen,T.D. and Livak,K.J. (2008) Analyzing real-time PCR data by the comparative C(T) method. *Nat. Protoc.*, **3**, 1101–1108.
18. Friel,N. and Pettitt,A.N. (2008) Marginal likelihood estimation via power posteriors. *J. R. Stat. Soc. B*, **70**, 589–607.
19. Girolami,M. and Calderhead,B. (2011) Riemann manifold Langevin and Hamiltonian Monte Carlo methods. *J. R. Stat. Soc. B*, **73**, 123–214.
20. Locke,J.C., Southern,M.M., Kozma-Bognar,L., Hibberd,V., Brown,P.E., Turner,M.S. and Millar,A.J. (2005) Extension of a genetic network model by iterative experimentation and mathematical analysis. *Mol. Syst. Biol.*, **1**, 2005.0013.
21. Calderhead,B. and Girolami,M. (2011) Statistical analysis of nonlinear dynamical systems using differential geometric sampling methods. *Interface Focus*, **1**, 821–835.
22. Hu,H.M., Zielinska-Kwiatkowska,A., Munro,K., Wilcox,J., Wu,D.Y., Yang,L. and Chansky,H.A. (2008) EWS/FLI1 suppresses retinoblastoma protein function and senescence in Ewing's sarcoma cells. *J. Orthop. Res.*, **26**, 886–893.
23. Hirata,M., Kugimiya,F., Fukai,A., Ohba,S., Kawamura,N., Ogasawara,T., Kawasaki,Y., Saito,T., Yano,F., Ikeda,T. *et al.* (2009) C/EBPbeta Promotes transition from proliferation to hypertrophic differentiation of chondrocytes through transactivation of p57. *PLoS One*, **4**, e4543.
24. Jackman,J. and O'Connor,P.M. (2001) Methods for synchronizing cells at specific stages of the cell cycle. In: Bonifacino,J.S., Dasso,M., Harford,J.B., Lippincott-Schwartz,J. and Yamada,K.M. (eds). *Curr. Protoc Cell Biol*. John Wiley & Sons, Inc, Hoboken, NJ , Chapter 8, Unit 8 3.
25. Henley,S.A. and Dick,F.A. (2012) The retinoblastoma family of proteins and their regulatory functions in the mammalian cell division cycle. *Cell Div.*, **7**, 10.
26. DeGregori,J. (2002) The genetics of the E2F family of transcription factors: shared functions and unique roles. *Biochim. Biophys. Acta*, **1602**, 131–150.
27. Hanahan,D. and Weinberg,R.A. (2000) The hallmarks of cancer. *Cell*, **100**, 57–70.
28. Mangan,S. and Alon,U. (2003) Structure and function of the feed-forward loop network motif. *Proc. Natl. Acad. Sci. U.S.A.*, **100**, 11980–11985.
29. Tirode,F., Laud-Duval,K., Prieur,A., Delorme,B., Charbord,P. and Delattre,O. (2007) Mesenchymal stem cell features of Ewing tumors. *Cancer Cell*, **11**, 421–429.
30. Lipinski,M., Braham,K., Philip,I., Wiels,J., Philip,T., Goridis,C., Lenoir,G.M. and Tursz,T. (1987) Neuroectoderm-associated antigens on Ewing's sarcoma cell lines. *Cancer Res.*, **47**, 183–187.
31. von Levetzow,C., Jiang,X., Gwye,Y., von Levetzow,G., Hung,L., Cooper,A., Hsu,J.H. and Lawlor,E.R. (2011) Modeling initiation of Ewing sarcoma in human neural crest cells. *PloS One*, **6**, e19305.
32. Tanaka,M., Yamazaki,Y., Kanno,Y., Igarashi,K., Aisaki,K., Kanno,J. and Nakamura,T. (2014) Ewing's sarcoma precursors are highly enriched in embryonic osteochondrogenic progenitors. *J. Clin. Invest.*, **124**, 3061–3074.
33. Freedman,J.A., Chang,J.T., Jakoi,L. and Nevins,J.R. (2009) A combinatorial mechanism for determining the specificity of E2F activation and repression. *Oncogene*, **28**, 2873–2881.
34. Li,Y., Zhang,D.Y., Ren,Q., Ye,F., Zhao,X., Daniels,G., Wu,X., Dynlacht,B. and Lee,P. (2012) Regulation of a novel androgen receptor target gene, cyclin B1, through androgen-dependent E2F family member switching. *Mol. Cell. Biol.*, **32**, 2454–2466.
35. Li,Y., Li,X., Fan,G., Fukushi,J., Matsumoto,Y., Iwamoto,Y. and Zhu,Y. (2012) Impairment of p53 acetylation by EWS-Fli1 chimeric protein in Ewing Family Tumors. *Cancer Lett.*, **320**, 14–22.
36. Rayman,J.B., Takahashi,Y., Indjeian,V.B., Dannenberg,J.H., Catchpole,S., Watson,R.J., te Riele,H. and Dynlacht,B.D. (2002) E2F mediates cell cycle-dependent transcriptional repression in vivo by recruitment of an HDAC1/mSin3B corepressor complex. *Genes Dev.*, **16**, 933–947.
37. Erkizan,H.V., Kong,Y., Merchant,M., Schlottmann,S., Barber-Rotenberg,J.S., Yuan,L., Abaan,O.D., Chou,T.H., Dakshanamurthy,S., Brown,M.L. *et al.* (2009) A small molecule blocking oncogenic protein EWS-FLI1 interaction with RNA helicase A inhibits growth of Ewing's sarcoma. *Nat. Med.*, **15**, 750–756.